Journal of Hazardous Materials 411 (2021) 125056

Contents lists available at ScienceDirect

Journal of Hazardous Materials

journal homepage: www.elsevier.com/locate/jhazmat

Metal-organic frameworks functionalized smart textiles for adsorptive removal of hazardous aromatic pollutants from ambient air

Hardeep Singh Jhinjer [a], Arunima Singh [b], Saswata Bhattacharya [b,*], Manjeet Jassal [a,*], Ashwini K. Agrawal [a,*]

[a] SMITA Research Lab, Department of Textile and Fibre Engineering, Indian Institute of Technology Delhi, Hauz Khas, New Delhi 110016, India
[b] Department of Physics, Indian Institute of Technology Delhi, Hauz Khas, New Delhi 110016, India

ARTICLE INFO

Editor: Dr. H. Artuto

Keywords:
ZIF MOFs
Smart textiles
VOCs/toxics adsorption
Air purification
DFT studies

ABSTRACT

Organic pollutants, with their increasing concentrations in the ambient air, are posing a severe threat to human health. Metal-organic frameworks (MOFs), due to their active functionalities and porous nature, have emerged as potential materials for the capture of organic pollutants and cleaning of the environment/air. In this work, the functionalization of cotton fabric is reported by the in-situ growth of zeolitic imidazolate framework (ZIF-8 and ZIF-67) MOFs on carboxymethylated cotton (CM Cotton) by employing a rapid and eco-friendly approach. The physicochemical characterization of the MOF functionalized fabrics (ZIF-8@CM Cotton and ZIF-67@CM Cotton) revealed uniform and wash durable attachment of porous ZIF nanocrystals on the surface of the fabric. These ZIF functionalized fabrics possessed high surface area and have been observed to adsorb significantly high concentrations of organic pollutants such as aniline, benzene, and styrene from ambient air. Interestingly these fabrics could be regenerated and reused repeatedly without any deterioration in their adsorption capacity. The negative and low binding energies calculated by DFT confirmed the physisorption of the aromatic pollutants on the surface of MOF functionalized fabrics. Such fabrics have a huge potential as protective textiles, anti-odor clothing, air purification filters, and related products.

1. Introduction

The increased levels of particulate matter, nitrous oxides, sulfur oxides, carbon oxides, and other toxic volatile organic compounds (VOCs) are of major concern for air pollution. These pollutants have adverse effects on human health (Kampa and Castanas, 2008). The presence of a small amount of these VOCs in the air can cause unpleasant odors and toxicity. Also, the long-term exposure to these pollutants, even at levels of few parts per million, can cause life-threatening respiratory diseases like asthma, eye and throat irritations, and even cancer (Soni et al., 2018).

The porous materials such as activated carbon, zeolites, and MOFs are the potential candidates for the capture of VOCs (Lashaki et al., 2012; Li et al., 2012; Takeuchi et al., 2012; Wang et al., 2004). Several MOFs such as MOF-199, ZIF-8, and ZIF-67, etc., and their hybrids are also reported in the literature for VOC adsorption (Saini and Pires, 2017; Vellingiri et al., 2017; Zhu et al., 2019). The MOFs, a new class of crystalline materials formed by extended coordination of metal ions and polydentate organic linkers, can be molecularly engineered for various applications. Depending on the nature of metal-linker interactions, MOFs with highly porous assemblies having fascinating properties, such as tailored/appropriate pore size and shape, active functionalities, and ultra-high surface area, can be obtained (Zhou et al., 2012). By virtue of these properties, a variety of MOFs has been explored for applications, such as adsorption, filtration, separation, catalysis, sensing, etc. (Furukawa et al., 2013; Li et al., 2016; Liu et al., 2014). Several groups have reported the MOF functional textiles and electrospun mats for various applications, which include antimicrobial, biomedical, particulate matter filtration, fuel filtration, chemical warfare protection, and anti UV radiation textiles (Abdelhameed et al., 2017; Emam and Abdelhameed, 2017; López-Maya et al., 2015; Lu et al., 2017; Neufeld et al., 2015; Rubin et al., 2018; Zhang et al., 2016). The reported methods for MOF and textile integration include the in-situ growth, layer by layer growth, and hot-pressing method (Chen et al., 2016; Y. Chen et al., 2017; da Silva Pinto et al., 2012; Lu et al., 2018). The reported methods have several limitations, such as the use of organic solvents, longer

* Corresponding authors.
E-mail addresses: saswata@physics.iitd.ac.in (S. Bhattacharya), manjeetjassal@gmail.com (M. Jassal), ashwini@smita-iitd.com (A.K. Agrawal).

https://doi.org/10.1016/j.jhazmat.2021.125056
Received 7 September 2020; Received in revised form 30 December 2020; Accepted 4 January 2021
Available online 9 January 2021

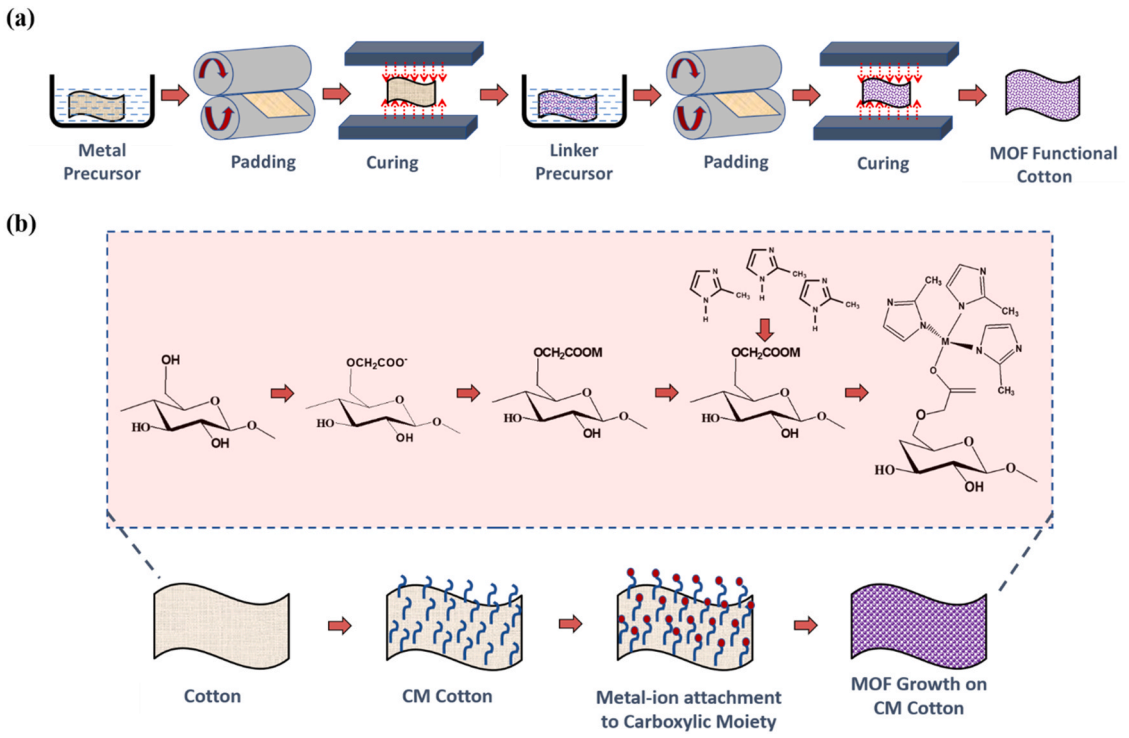

Fig. 1. (a) Schematic diagram of the experimental procedure of in-situ growth of ZIF-8 and ZIF-67 MOF on CM Cotton fabric. (b) Schematic of the growth mechanism of ZIF-8 and ZIF-67 MOF on CM Cotton fabric.

reaction durations, poor washing durability, and use of high temperatures (not suitable for textile fibers), which ultimately restricts their upscaling.

ZIFs are the class of MOF materials in which transition metal ions (Fe, Co, Cu, and Zn) are tetrahedrally-coordinated to the imidazolate linkers and has a structural resemblance to Zeolites. ZIF MOFs possess excellent moisture and thermal stability as compared to the other carboxylate linker-based MOFs (Phan et al., 2010). ZIF-8 and ZIF-67 are two MOF materials that belong to the class of ZIF MOFs. ZIF-8 and ZIF-67 are composed of 2-methylimidazole linkers tetrahedrally connected, respectively, with Zn (ZIF-8) and Co (ZIF-67) to make sodalite-type cage structures (Zhou et al., 2017). There are many reported applications of ZIF-8 in catalysis, sensing, gas storage, hydrocarbon separation, etc. (Hu et al., 2013; Lu and Hupp, 2010; Pan and Lai, 2011; Tran et al., 2011). ZIF-67 has also been explored for different applications such as sensing, catalysis, energy storage, etc. (Tu et al., 2015; Yang et al., 2015; Zhou et al., 2018). These materials have also been analyzed by many computational methods in diverse applications such as adsorption and separation of gas mixtures (Hobday et al., 2018; Krokidas et al., 2017). Among these, Density Functional Theory (DFT) is a quantum mechanical method, i.e., based on first-principles, that provides a viable prediction of the energetics of a specific geometry.

In the present study, the in-situ growth of ZIF-8 and ZIF-67 nanocrystals on the carboxymethylated cotton fabric is reported using a rapid water-based textile finishing approach. The surface characteristics of the fabrics in terms of surface morphology, surface area, pore size, and nature of chemical groups were investigated. The VOC adsorption capacity of MOF functionalized fabrics for aromatic pollutants, such as aniline, benzene, and styrene, were determined by UV-Visible spectroscopy, and the adsorption behavior is explained by DFT calculations. The ZIF-8@CM Cotton and ZIF-67@CM Cotton were the codes assigned to the ZIF-8 and ZIF-67 functionalized CM Cotton, respectively.

2. Experimental section

2.1. Materials used

Zinc nitrate hexahydrate (≥99%), 2-methylimidazole (≥ 99.0%) were procured from Sisco Research Laboratories Pvt. Ltd, New Delhi. Cobalt nitrate hexahydrate (≥ 97.0%), sodium hydroxide (>97%), and sodium monochloroacetate (≥ 98.0%) were purchased from Central Drug House Pvt. Ltd, New Delhi. Aniline (≥ 99.5%), benzene (≥ 99.8%), triethylamine (≥ 99.5%), and methanol (≥ 99.8%) were supplied by Merck Life Sciences Pvt. Ltd. Mumbai. Styrene was purchased from Tokyo Chemical Industry (TCI) Co. Ltd., Japan. A ready to dye cotton fabric having a GSM of 114 g/m^2 was supplied by Surya Processors Private Limited, Ghaziabad, India. The nylon syringe filters of size 0.2 μm were procured from Axiva, Delhi.

2.2. Carboxymethylation of cotton fabric

The cotton fabric was scoured before carboxymethylation (CM) in 3 g/l non-ionic detergent and 0.5 g/l sodium carbonate solution at 50 °C for 1 h to remove all the impurities. The fabric was kept at substrate mass to bath liquor ratio of around 1:30 (w/v) for the scouring of the fabric. Further, the carboxymethylation of the fabric was achieved by reacting 1 M sodium monochloroacetate in 5% aq. NaOH at 70 °C for 1 h. The fabric mass to liquor ratio was kept at 1:30 (w/v). Finally, the fabric was rinsed several times to remove all the detergent and alkali. The fabric was soaked in a 2 g/l solution of acetic acid for 10 min to neutralize the effect of the remaining alkali. The fabric was thoroughly rinsed and dried in stenter at 80 °C for 10 min

2.3. Calculation of CM content and degree of substitution (DS)

The content of CM was calculated by immersing a 5 × 5 cm^2 specimen of cotton fabric in 100 ml of 0.5% HCl solution for 16 h (Kuma et al., 2018). The fabric was rinsed in water several times to remove the HCl completely, and it was confirmed by a silver nitrate drop test. The

fabric was dried at room temperature (~28 °C), and 0.25 g of fabric was placed in 25 ml of 0.05 N solution of NaOH for 4 h in a sealed container under a nitrogen blanket to prevent the reaction of NaOH with environmental carbon dioxide. A blank solution of 25 ml 0.05 N NaOH was considered as control. After 10 h, the NaOH solutions were titrated with 0.05 N HCl using phenolphthalein as an indicator. The amount of the titrant used for each sample was recorded carefully, and the carboxymethylation content (CM content) and degree of substitution (DS) were calculated by using the following equations:

$$CM\ Content\left(\frac{mmol}{100\ g}\right) = 100(Vo - Vs).\frac{N}{wt.\ of\ fabric\ in\ grams} \quad (1)$$

$$DS = \frac{CM\ Content\left(\frac{mmol}{100\ g}\right) \times 162\ g/mol}{1000\left(\frac{mmole}{mol}\right) \times 100\ g} \quad (2)$$

Where 162 g/mol is the molecular weight of an anhydrous glucose unit. Finally, from Eqs. (1) and (2), the CM Content was found to be around 8.2 mmole/100 g of fabric, and the subsequent DS was around 0.013. In Eq. (1), V_o denotes the volume of HCl used for titration of a blank solution, V_s is the volume of HCl used for titration of the sample solution, and N indicates the normality of the HCl titrant.

2.4. In-situ growth of ZIF-8 and ZIF-67 MOFs on CM Cotton

The parameters for the functionalization of CM Cotton were varied to determine the optimum values required to give a desirable add-on of MOF. The growth of ZIF-8/ZIF-67 on carboxymethylated cotton (CM Cotton) was carried out by immersing the fabric in a 0.2 M metal precursor solution (zinc nitrate hexahydrate for ZIF-8 or cobalt nitrate hexahydrate for ZIF-67) for 1 min followed by padding at 1.8 bar (at an expression of ~ 80%) and curing/drying at 150 °C in stenter for 1 min. Then the fabric was immersed in a 0.8 M 2-methylimidazole solution for one minute, followed by padding, drying, and curing. The molarity of the linker precursor solution was four times higher as compared to the metal precursor to facilitate the small and rapid crystal growth of the MOF crystals. The whole procedure was repeated to increase the add-on of MOF on fabric. A small volume of triethylamine (TEA) was added to the 2-methylimidazole precursor solution for the deprotonation (Nordin et al., 2014). After the growth procedure, the fabrics were washed by a vigorous rinsing in water for at least three times for 5 min followed by rinsing in methanol to remove all the weakly attached MOF on the surface of the fabric. The fabrics were dried in a vacuum oven at 85 °C for 4 h. All characterizations and aromatic pollutant capture studies were performed after the washing and drying of the fabrics. The schematic of the growth procedure is shown in Fig. 1(a). Fig. 1(b) shows the schematic mechanism of MOF growth on CM fabric. The ZIF-8@CM Cotton and ZIF-67@CM Cotton were the codes assigned to the ZIF-8 and ZIF-67 functionalized CM Cotton, respectively.

2.5. Characterization

The morphological and EDX analysis were carried out by JEOL JSM-7900F FESEM and Oxford IE 250 X Max 150 EDX spectrometer, respectively. The functional group studies were performed by the Nicolet iS50 FTIR system with diamond ATR from Thermo Scientific. The XRD patterns were recorded by Rigaku Ultima IV, Ri X-ray diffractometer at a scan rate of 2°/min. The surface area measurements were carried out at 77.3 K by Micromeritics Gemini V surface area analyzer, and all the samples were degassed at 95 °C for 8 h before surface area measurement. The surface chemistry was analyzed by Scienta Omicron X-ray photoelectron spectroscopy (XPS) with monochromatic aluminum K_α X-rays having photon energy of 1486.7 eV. Agilent 7900 system ICP MS system was used to calculate the metal content to estimate the add on of MOF on fabric by digesting the fabric in aqua regia. The adsorption experiments for the quantification of aromatic pollutant adsorption were performed using Perkin Elmer Lambda 35 spectrophotometer. The thermographic studies were performed under nitrogen in the range of 50 °C to 750 °C at a heating rate of 20 °C/min using the Perkin Elmer TGA 4000 analyzer.

2.6. Stability studies of the fabric

The stability studies were carried out by immersing the MOF functionalized fabrics in a water bath for 24 h, followed by XRD analysis.

2.7. Gas-phase aromatic pollutant capture studies

2.7.1. Time-dependent pollutant capture studies at high pollutant concentrations

The aromatic pollutant capture studies by MOF functionalized CM Cotton, and CM Cotton were performed in 20 ml glass vials at ambient temperature (~ 25–30 °C). The vials were charged with 300 µl of aromatic pollutant and left for 30 min for equilibration. The 25 mg of the cotton fabric was hung in the headspace of the vial without touching the pollutant at the bottom for a given period. The vial was closed and sealed properly. After a given interval of time, the fabric was removed from the vial and kept under an active vacuum for half an hour. Finally, the fabric was soaked in 4 ml of methanol for 2 h. The methanol solution was filtered using a 0.2 µm syringe filter and analyzed by UV–visible spectroscopy to estimate the captured pollutant. All the experiments were done in triplicate and performed using three model aromatic pollutants-aniline, benzene, and styrene. These studies were performed to calculate the maximum adsorption capacity of the MOF functional fabrics.

2.7.2. Pollutant capture studies at harmful environmental concentrations

The performance of MOF functionalized fabrics was also tested under realistic toxic environmental concentrations (around 500 ppm). The low concentration pollutant capture experiments were performed in 22 ml plastic vials at ambient temperature (~ 25–30 °C). The 25 mg fabric was kept inside the vial, and the desired amount of stock solution of the aromatic pollutant in ethanol was inserted on the walls of the vial carefully to make an overall concentration of 500 ppm inside the vial volume. The vial was sealed properly and kept at 80 °C for 15 min to generate pollutant vapors inside the vial. After 2 h, the fabric was removed from the vial and soaked in 4 ml of methanol for half an hour. The methanol solution was filtered by Whatman 0.2 µm syringe filter and analyzed by UV–visible spectroscopy to estimate the captured pollutants. All the experiments were performed in triplicate with three gases, aniline, benzene, and styrene, as model pollutants.

2.7.3. Desorption

The desorption studies by MOF@CM Cotton and CM Cotton were performed at 120 °C as a function of time in an oven at ambient pressure. First, 25 mg of fabrics were exposed to the aniline vapors for 1 h, as explained above in Section 2.7.1 of the pollutant capture studies. After that, the fabric was removed from the vial and kept at 120 °C for a defined period. Finally, the fabric was soaked in 4 ml of methanol for 2 h. The methanol solution was filtered by a 0.2 µm syringe filter and analyzed by UV–visible spectroscopy to estimate the remaining aniline. All the experiments were carried out in triplicate.

2.7.4. Reusability and recyclability

The reusability or regeneration of the functionalized fabrics was investigated by carrying out the pollutant capture studies for 1 h as per the procedure given in section (a) above. The same procedure was repeated for two more cycles on the same fabric. All the experiments were performed in triplicate with all three aromatic compounds- aniline, benzene, and styrene.

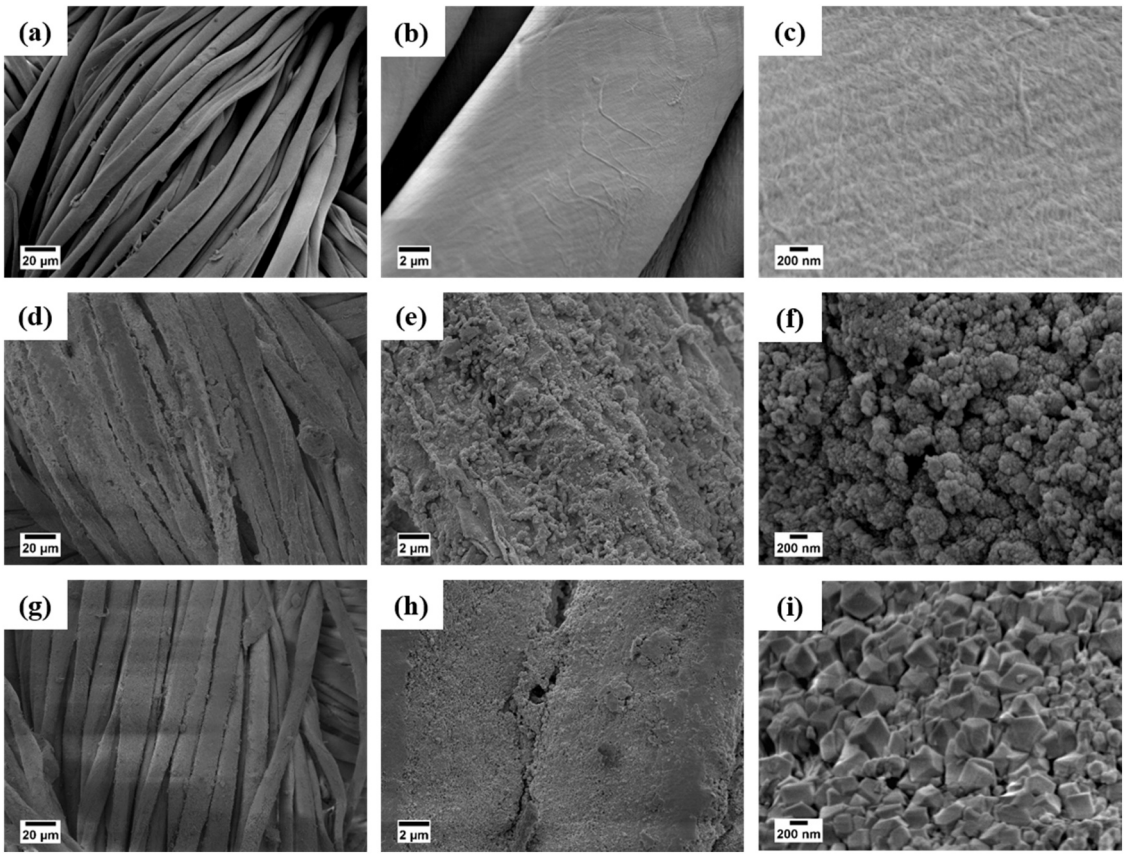

Fig. 2. FESEM micrographs at different magnifications of (a to c) CM Cotton fabric, (d to f) ZIF-8@CM Cotton fabric, (g to i) ZIF- 67@CM Cotton fabric.

2.8. Computational Studies

Density functional theory (DFT) calculations were performed using the Vienna ab initio Simulation Package (VASP) with the projected augmented wave (PAW) potential (Hohenberg and Kohn, 1964; Kohn and Sham, 1965; Kresse and Furthmüller, 1996; Phys. Rev. B 50, 17953 (1994) – Projector augmented-wave method, n.d.). The Perdew–Burke–Ernzerhof (PBE) exchange-correlation functional within the generalized gradient approximation (GGA) was used in all the calculations (Perdew et al., 1996). The cut-off energy of 500 eV was chosen for the plane-wave basis set. The tolerance energy for the convergence was set to 0.001 meV to achieve self-consistency in the total energy. All the electronic configurations were fully relaxed until the ionic forces were smaller than 0.01 eV/Å using conjugate gradient minimization. Van der Waals interaction was also considered by employing the Tkatchenko-Scheffler van der Waals correction scheme (Tkatchenko and Scheffler, 2009). The ZIF-8 and ZIF-67 primitive cells with 138 atoms have been modeled with a different number of aromatic rings (Knebel et al., 2017). Their corresponding binding energies direct towards the type of adsorption in the system.

3. Results and discussion

The parameters for the functionalization of CM Cotton were varied to determine the optimum values required to give a desirable add-on of ZIF-8. For this, the effect of TEA, ratio of metal to linker, and the concentration of metal were studied. The results are shown in Table S1 in the Supplementary Information. It may be observed that an M:L:T ratio of 1:4:2 gave the nano-sized growth of MOF particles with high wash durability and an optimum add-on of MOF at around 12 wt%. A similar trend was also observed for ZIF-67. The add-on values were at kept in this range to retain the flexibility and drape of the functionalized fabric.

3.1. Surface morphology and structural investigation of ZIF-8@CM Cotton and ZIF-67@CM Cotton fabrics

The in-situ growth of MOF crystals on the CM Cotton was carried out as per the scheme shown in Fig. 1(a), and Fig. 1(b) shows the mechanism of MOF growth on fabric. The carboxymethylation of the fabric provided the anionic carboxylate sites on the cotton fabric. On immersion in the metal precursor, the metal ions were ionically bonded to the carboxylate anions. It offered the anchoring step for the growth of MOF on the cotton fabric. The immersion of this fabric in the linker precursor solution completed the growth of MOF. The padding process helped in uniform distribution of precursors, removal of extra precursor solution, and the curing process facilitated the growth of ZIF crystals on the surface of cotton rather than in the solution. It was also observed that the MOFs covered nearly 100% surface of the cotton fabric and were uniformly formed all over the entire fabric surface.

The formation of small size may be attributed to an extremely fast nucleation rate in an aqueous medium. The deprotonation of the linker by a strong base, i.e., TEA, helped in boosting the growth rate on the fabric by capturing the acidic hydrogen from 2-methylimidazole. The curing step also played an essential role in solvent evaporation and ultimately restricting the growth of MOFs to smaller crystals. The carboxymethylation of the fabric and the formation of the smaller size crystals contributed to the improved washing durability of the MOF functionalized fabrics.

Fig. 2 shows the FESEM micrographs of the CM Cotton (a to c), ZIF-8@CM Cotton (d to f), and ZIF-67@CM Cotton (g to i). The FESEM analysis showed the uniform growth of ZIF-8 and ZIF-67 crystals over the surface of CM Cotton. The size of the MOF crystals was observed to be in the range of a few hundred nanometers. However, it was difficult to calculate the crystal size from FESEM micrographs because MOF crystals were uniformly packed on the fabric surface and were in the form of

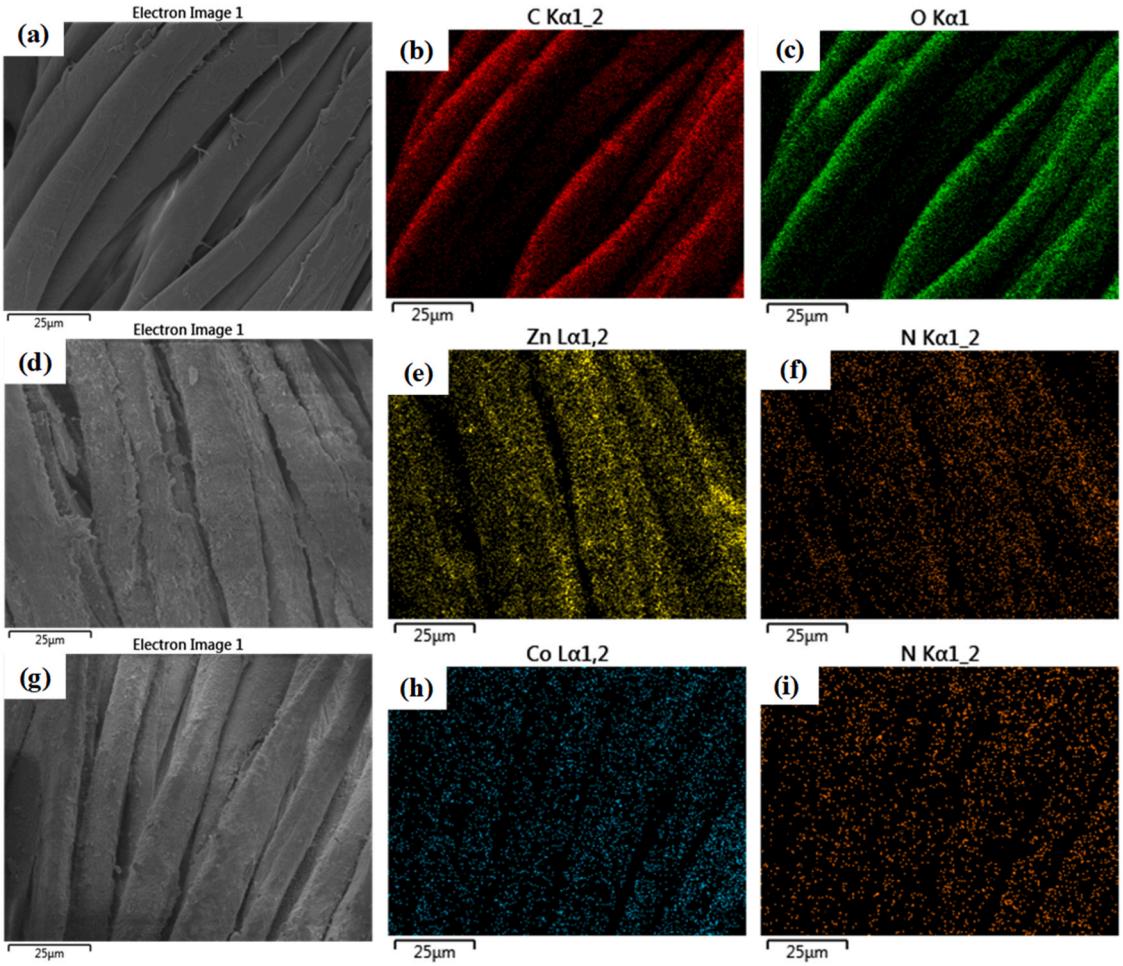

Fig. 3. (a) Electron image of CM Cotton fabric. (b) Carbon mapping of CM Cotton fabric. (c) Oxygen mapping of CM Cotton fabric. (d) Electron image of ZIF-8@CM Cotton fabric. (e) Zinc mapping of ZIF-8@CM Cotton fabric. (f) Nitrogen mapping of ZIF-8@CM Cotton fabric. (g) Electron image of ZIF-67@CM Cotton fabric. (h) Cobalt mapping of ZIF-67@CM Cotton fabric. (i) Nitrogen mapping of ZIF-67@CM Cotton fabric.

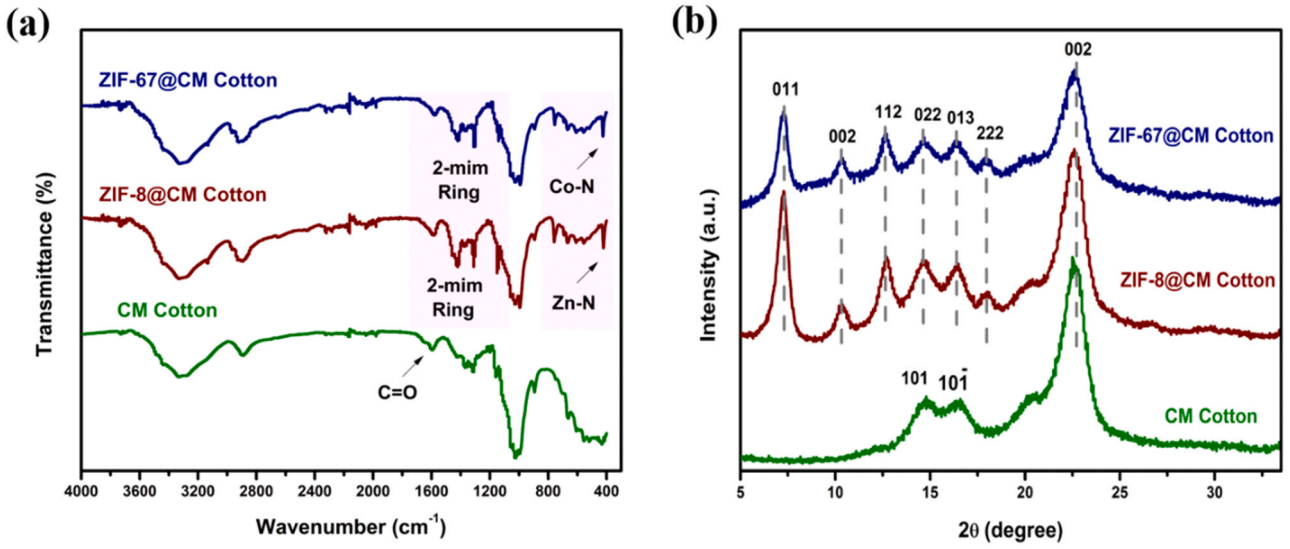

Fig. 4. (a) ATR FTIR spectra of CM Cotton, ZIF-8@CM Cotton, and ZIF-67@CM Cotton fabric, (b) XRD Spectra of CM Cotton, ZIF-8@CM Cotton, and ZIF-67@CM Cotton fabrics.

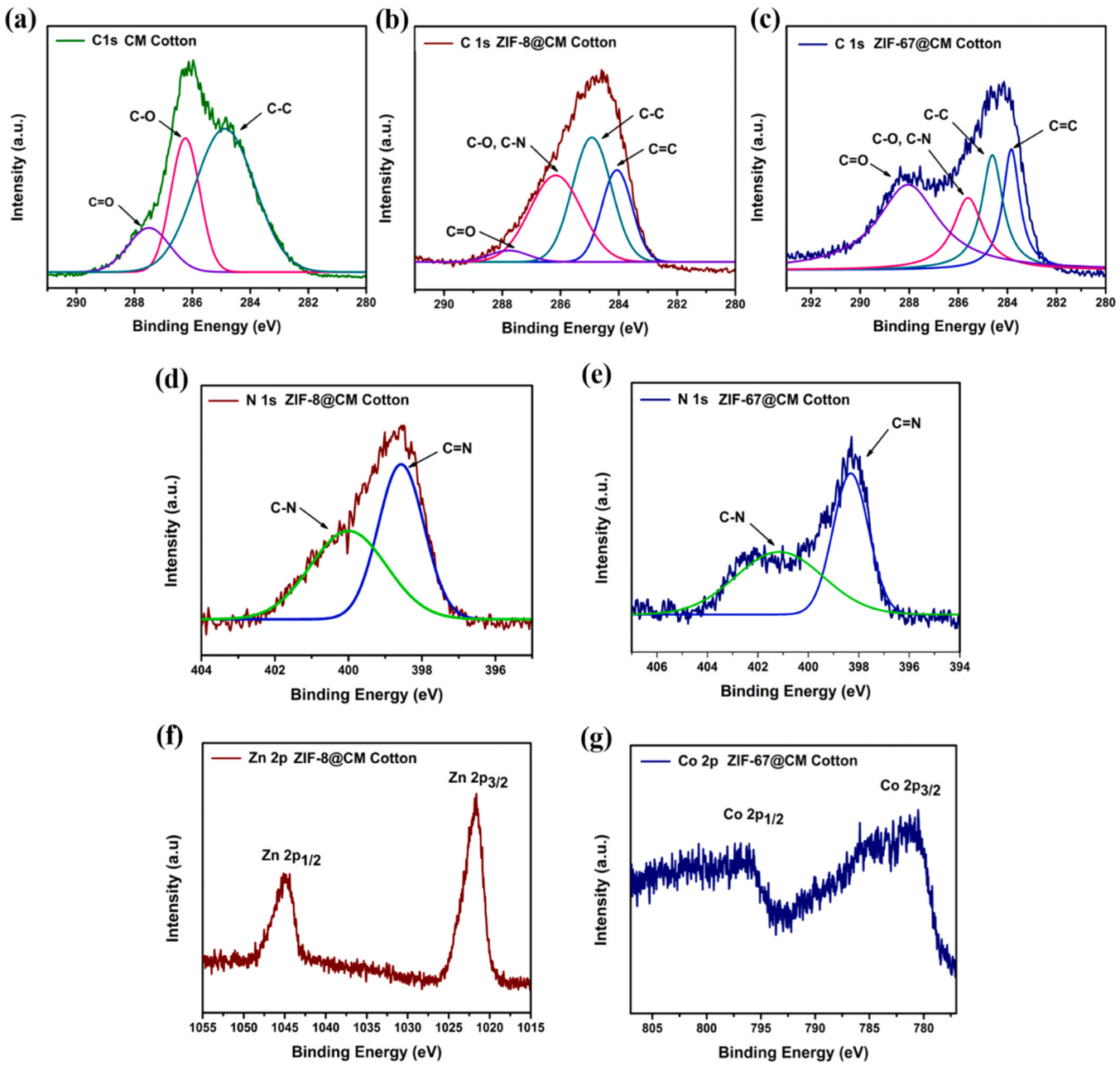

Fig. 5. High-resolution XPS C1s spectra of (a) CM Cotton fabric, (b) ZIF-8@CM Cotton fabric, and (c) ZIF-67@CM Cotton fabric. High-resolution XPS N 1s spectra of (d) ZIF-8@CM Cotton fabric, and (e) ZIF-67@CM Cotton fabric. (f) High-resolution XPS Zn 2p spectra of ZIF-8@CM Cotton fabric. (g) High-resolution XPS Co 2p spectra of ZIF-67@CM Cotton.

aggregates. The shape of the ZIF-8 crystals grown on the fabric was not completely spherical. They had indistinct hexagonal features. On the other hand, the ZIF-67 crystals had cubic and tetragonal shapes. The washing durability studies of the MOF functionalized fabrics were also evaluated following the AATCC 1 A washing protocol, which is equivalent to 5 laundry cycles. The FESEM images of washed fabrics are shown in Fig. S2 in the Supplementary Information. As can be observed from the FESEM micrographs that even after two such washing cycles (i.e., 10 laundry washes), the fabric surface was still uniformly covered with the MOFs.

It showed that the reported fabrics are highly durable to washing. Fig. 3 shows the EDX mapping of CM Cotton (a to c), ZIF-8@CM Cotton (d to f), and ZIF-67@CM Cotton (g to i) fabrics. From the mapping of Zn (Fig. 3(e)) and N (Fig. 3(f)), it can be observed that both these elements are uniformly distributed over the entire surface. This confirmed the complete surface coverage of the fabric by ZIF-8 MOF crystals. The mapping of N corresponds to the organic linker 2-methylimidazole. Similarly, results were also observed from the mapping of Co and N in ZIF-67@CM Cotton (Fig. 3(h) and 3(i)). The mapping results are in conformance with the SEM analysis.

Further, the surface functional groups were analyzed by ATR FTIR spectroscopy. Fig. 4(a) depicts the ATR FTIR spectra of CM Cotton, ZIF-8@CM Cotton, and ZIF-67@CM Cotton. The adsorption band at 1590 cm^{-1} corresponds to the carboxylic acid group introduced on the cellulosic chain. As we mentioned earlier that the CM content was ~8.2 mmole/100 g of fabric, and the subsequent degree of substitution (DS) was 0.01328. The other bands observed at 3320 cm^{-1} and 2890 cm^{-1} are assigned to the stretching of hydroxyl groups and C–H stretching vibration of cotton, respectively. The bands at 1340 cm^{-1}, 1030 cm^{-1}, and 890 cm^{-1} confirmed the deformation vibrations of the C–H groups,

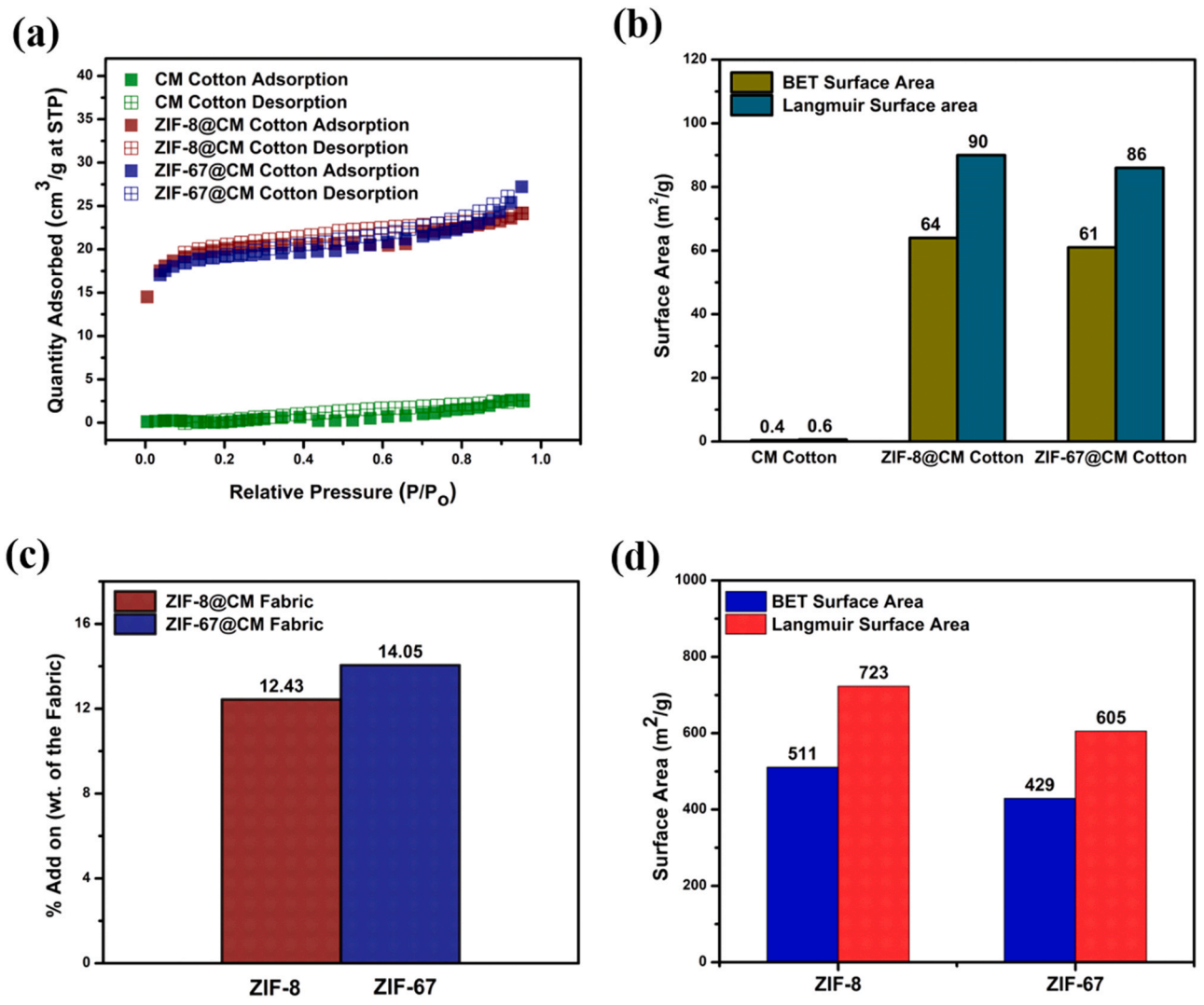

Fig. 6. (a) N_2 adsorption and desorption isotherms of CM Cotton, ZIF-8@CM Cotton, and ZIF-67@CM Cotton fabrics. (b) Bar graphs of calculated BET and Langmuir surface areas of CM Cotton, ZIF-8@CM Cotton, and ZIF-67@CM Cotton fabrics. (c) Bar graph depicting percentage add-on (from ICP-MS) of ZIF-8 and ZIF-67 MOF crystals on ZIF-8@CM Cotton and ZIF-67@CM Cotton fabrics, respectively, on the weight of the fabrics. (d) Bar graph showing the total effective surface areas of ZIF-8 and ZIF-67 MOF crystals grown on CM Cotton fabrics.

–C–O groups, and β-glycosidic linkage between glucose units of cotton, respectively. The presence of IR adsorption bands in MOF functionalized cotton at 1580 cm^{-1} confirmed the C=N stretching, and the bands at 1420 cm^{-1}, 1310 cm^{-1}, and 1140 cm^{-1} confirmed the stretching vibrations of the 2-methylimidazole ring (2-mim Ring). Additionally, the presence of a band at 746 cm^{-1} corresponds to the aromatic C–H bending of the 2-methylimidazole ring. The absorption band associated with the Metal–N stretching was observed at 420 cm^{-1} in ZIF-8@CM Cotton and at 430 cm^{-1} in ZIF-67@CM Cotton. The ATR FTIR analysis confirmed the formation of ZIF-8 and ZIF-67 MOF crystals on the surface of CM Cotton.

Further, the crystal structures of ZIF-8 and ZIF-67 MOFs grown on the fabric were studied with X-ray diffraction. The spectra obtained are shown in Fig. 4(b). The X-ray diffraction pattern of CM Cotton fabric had the three diffraction peaks at 2θ values of 14.87°, 16.6°, and 22.5°, which correspond to the (1 0 1), (1 0 -1), and (0 0 2) planes of cellulose, respectively. The XRD diffraction pattern of ZIF-8@CM Cotton showed the characteristic diffraction peaks of ZIF-8 at 2θ values of 7.3° (0 1 1), 10.4° (0 0 2), 12.6° (1 1 2), 14.6° (0 2 2), 16.4° (0 1 3), and 18.0° (2 2 2). Similarly, the diffraction peaks corresponding to ZIF-67 were also observed in the XRD pattern of ZIF-67@CM Cotton fabric. The X-ray diffraction patterns supported the formation of tetrahedron ZIF-8 and ZIF-67 MOF crystals on the surface of the fabric, and the results are in agreement with the reported literature (Zhou et al., 2017).

Further, the surface chemistry of the MOF functionalized cotton fabrics was studied with the help of XPS. Fig. 5(a) depicts the high-resolution C 1s spectrum of CM Cotton. The presence of binding energy peaks at 287.49 eV, 286.24 eV, and 284.87 eV confirmed the C=O, C–O, and C–C bonding of cellulose. C=O corresponds to the carboxylic moieties of CM Cotton and C–C and C–O to the cellulosic structure. As shown in Fig. 5(b), the binding energy peaks in the C 1s spectrum of ZIF-8@CM Cotton observed at 286.16 eV and at 284.06 eV are associated with the C–N and C=C bonding of 2-methylimidazole ring of ZIF-8 MOF. Similarly, C 1s spectra of ZIF-67@CM Cotton (Fig. 5(c)), also shows the presence of these two peaks with binding energies of 285.60 eV and 283.84 eV, respectively.

Fig. 5(d) demonstrates the N 1s spectra of ZIF-8@CM Cotton. The binding energy peaks at 399.99 eV, and 398.56 eV is assigned to the C–N and C=N bonding, characteristic of the 2-methylimidazole ring of ZIF-8. As expected, the N 1s spectra of ZIF-67@CM Cotton also confirmed the presence of C-N and C=N bonding of 2-methylimidazole ring at binding energies of 401.14 eV and 398.31 eV, respectively (Fig. 5(e)). Fig. 5(f) and (g) show the Zn 2p XPS spectra of ZIF-8@CM fabric and the Co 2p spectra of ZIF-67@CM fabric, respectively. The Zn $2p_{½}$ peak at

Table 1
Comparison of N_2 surface areas and pore size of functionalized cotton fabrics.

S. No.	Parameter	ZIF-8@CM Cotton	ZIF-67@CM Cotton
1.	Single point surface area at P/Po = 0.300 (m^2/g)	62	59
2.	BET surface area (m^2/g)	64	61
3.	Langmuir surface area (m^2/g)	90	86
4.	External surface area (m^2/g)	16	11
5.	Pore volume (cm^3/g)	2.3×10^{-2}	2.4×10^{-2}
6.	Adsorption average pore size (Å)	23	27

1045 eV and $2p_{3/2}$ peak at 1021.60 eV confirmed the presence of the Zn metal center of ZIF-8 MOF in ZIF-8@CM Cotton. Similarly, the Co $2p_{½}$ peak at 796.68 eV and $2p_{3/2}$ peak at 781.78 eV indicated that Co metal was present as a center in ZIF-67 MOF. The XPS analysis confirmed the growth of ZIF-8 and ZIF-67 MOFs on the surface of the cotton fabric.

Fig. 6(a) demonstrates N_2 adsorption and desorption plots of CM Cotton, ZIF-8@CM Cotton, and ZIF-67@CM Cotton fabrics. The N_2 adsorption isotherms of MOF functionalized fabrics confirmed the microporous nature of the MOF functionalized fabrics. This suggested that the micropores of MOF crystals grown on the fabric were accessible for the adsorption of N_2. Further, the BET surface areas of CM Cotton, ZIF-8@CM Cotton, and ZIF-67@CM Cotton were found to be 0.4 m^2/g, 64 m^2/g, and 61 m^2/g, respectively. Apart from the BET surface area, Langmuir surface areas of CM Cotton, ZIF-8@CM Cotton, and ZIF-67@CM Cotton were observed to be 0.6 m^2/g, 90 m^2/g, and 86 m^2/g, respectively. It may be noted that very low values of surface areas of CM cotton as determined by BET experiments suggest that the substrate does not contain micro or mesopores and maybe mostly composed of macroporous structure, which cannot be determined using BET experiment. However, the high values of the surface area of functionalized CM cottons show that the cotton substrates could be successfully modified to contain a large amount of micro & mesopores.

A comparative bar graph that illustrates the BET and Langmuir surface areas of the CM Cotton, ZIF-8@CM Cotton, and ZIF-67@CM Cotton is shown in Fig. 6(b). Apart from BET and Langmuir surface areas, Table 1 also presents the measured external surface area and pore size of the tested samples. The external surface areas of ZIF-8@CM Cotton and ZIF-67@CM Cotton samples were 16 m^2/g and 11 m^2/g, respectively. Pore sizes in the cases of ZIF-8@CM Cotton and ZIF-67@CM Cotton were 23 A° and 27 A°, respectively. These pore sizes were found to be a little different from the pore sizes of ZIF-8 and ZIF-67 powders, which are reported to be approximately 13 A° in the literature (Zhou et al., 2017). In a recent study, it has been suggested that 2-methylimidazole linkers are quite mobile and can twist to adjust the pore

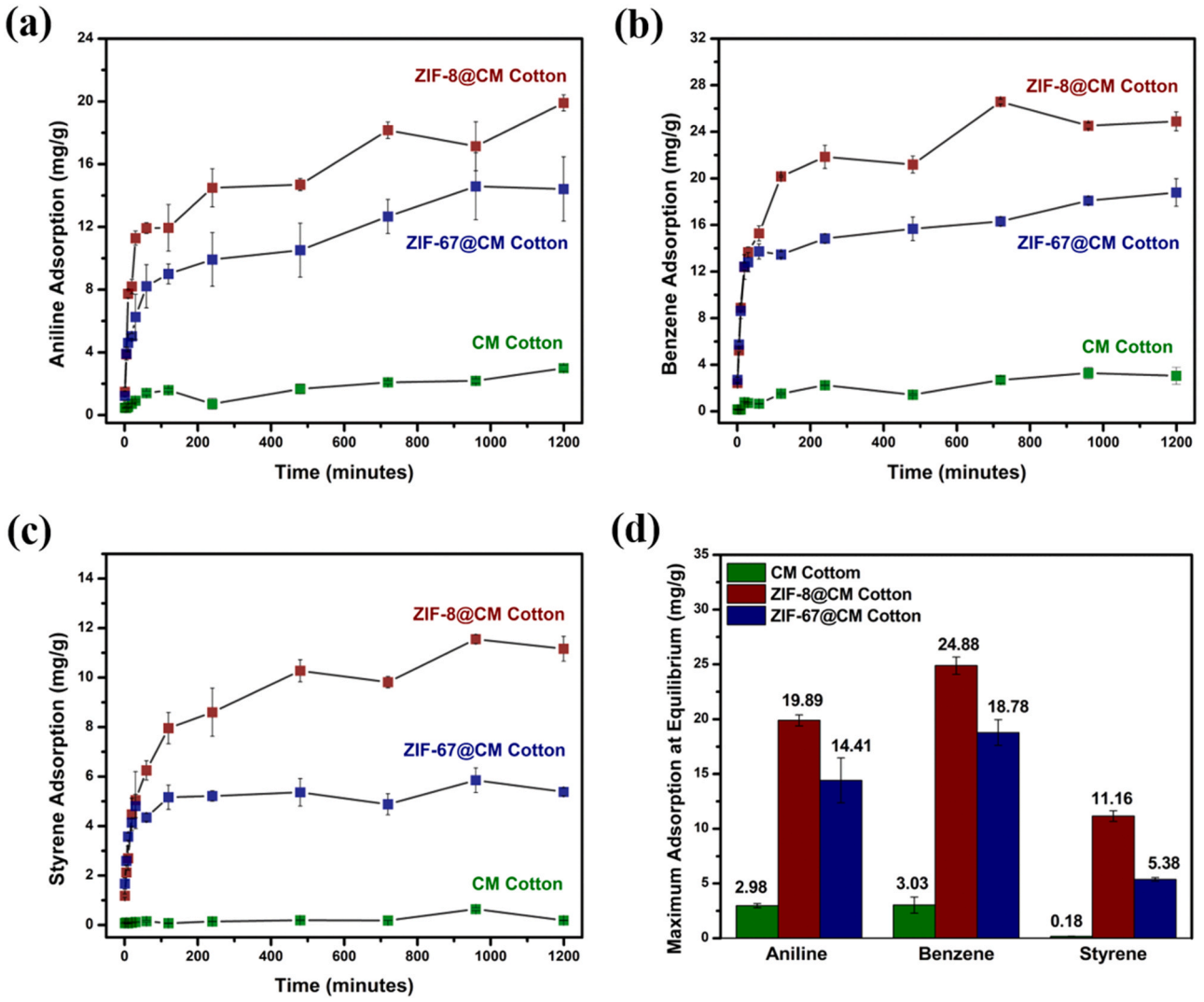

Fig. 7. Time-dependent high concentration adsorption plots of (a) aniline (b) benzene (c) styrene by CM Cotton, ZIF-8@CM Cotton, and ZIF-67@CM Cotton fabrics. (d) Bar graphs depicting the observed maximum capture of aromatic pollutants by CM Cotton, ZIF-8@CM Cotton, and ZIF-67@CM Cotton fabrics at equilibrium.

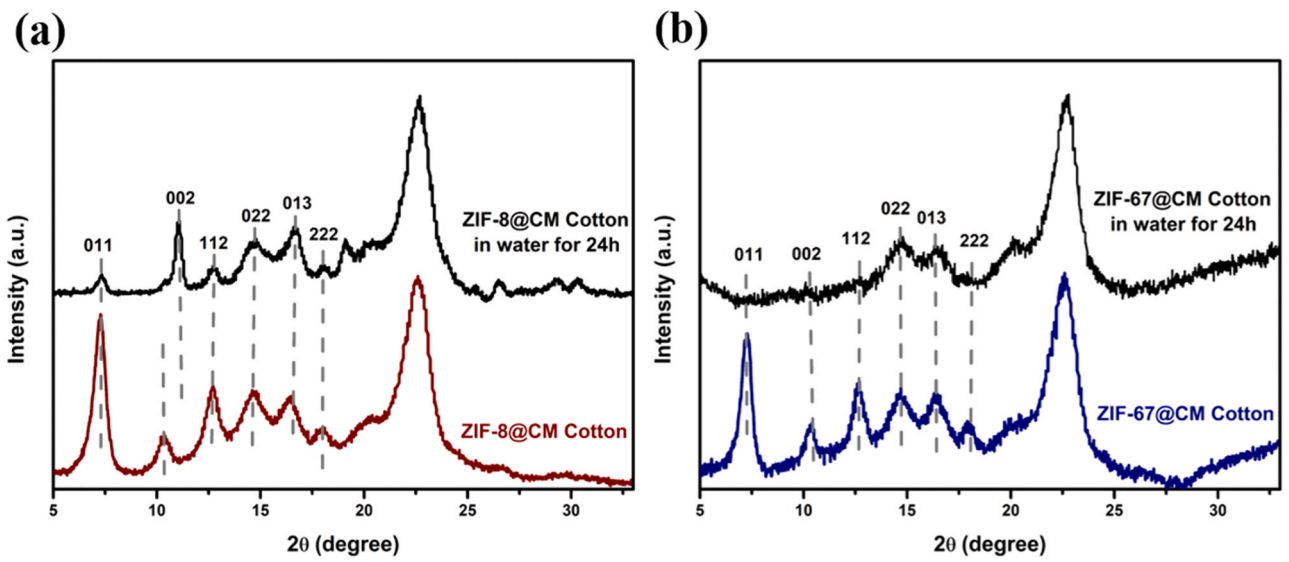

Fig. 8. XRD spectra of (a) ZIF-8@CM Cotton fabric before and after immersion in the water bath for 24 h. (b) ZIF-67@CM Cotton fabrics before and after immersion in the water bath for 24 h.

sizes (Kolokolov et al., 2015). The integration of MOFs with the carboxymethyl groups of CM Cotton may be responsible for these changes.

The ICP-MS studies were further performed to calculate the add on of MOFs on the fabric based on metal content (Zn or Co) (Fig. 6(c)). It was found that the add-ons of ZIF-8 and ZIF-67 were around 12.43% and 14.05% (on the weight of fabric), respectively, based on the Zn and Co contents. In order to investigate the microporosity developed within the MOF structures grown on the fabric, the effective surface area of MOF crystals of ZIF-8 and ZIF-67 present on the fabrics were calculated from add-ons and N_2 adsorption analysis of the functionalized samples (Fig. 6 (d)). It was found that ZIF-8 MOF could show a large BET surface area of 511 m^2/g and Langmuir surface area of 723 m^2/g based on MOF weight. Similarly, ZIF-67 MOF had the BET surface area of 429 m^2/g and Langmuir surface area of 605 m^2/g based on MOF weight. These analyses showed that ZIF-8 MOF possessed a larger surface area as compared to ZIF-67 MOF. However, in the literature, the reported BET and Langmuir surface areas of the two, i.e., ZIF-8 and ZIF-67, are similar and higher in the range of 1800–2000 m^2/g (Zhou et al., 2017).

This difference might be due to the fact that in the treated fabric, the surface area of MOFs grown on the surface of the fabric may not be fully accessible to the N_2 gas due to the compact deposition of crystals on the fabric surface. Moreover, the surface areas of the MOFs are highly dependent on the synthesis conditions, crystal size, etc. In the present study, a pad-dry-cure method has been adopted for the rapid growth of the MOFs to target the commercial viability of the process. This method may have resulted in the formation of compact small-sized MOFs with an effective lower surface area than freely synthesized MOF powders.

3.2. Aromatic pollutants capture studies

The three aromatic VOCs viz. aniline, benzene, and styrene were selected as model pollutants for the study. Two sets of experiments were designed to evaluate the performance of MOF functional fabrics for the capture of pollutants at ambient conditions. The first set of experiments was performed at high concentrations of aromatic pollutants to assess the maximum adsorption capacities of all the MOF@ CM Cotton fabrics.

Fig. 7 shows the high concentration adsorption results of three pollutants on CM Cotton, ZIF-8@CM Cotton, and ZIF-67@CM Cotton fabric at ambient temperature and pressure. The pollutant adsorption is plotted as mg/g (milligrams of pollutant per gram of the fabric sample). The control fabric, i.e., the CM Cotton, adsorbed 0.46 mg/g of aniline in one minute (Fig. 7(a)), while ZIF-8@CM Cotton and ZIF-67@CM Cotton captured about 1.47 mg/g and 1.21 mg/g of aniline, respectively. The adsorption rate in the control fabric was very slow, and even after 20 h, it adsorbed just 2.98 mg of aniline per gram of the fabric. On the contrary, the rate of adsorption of aniline was quite fast on MOF functionalized fabrics. In the first 30 min, the adsorption rate of aniline was 11.27 mg/g and 6.25 mg/g for ZIF-8@CM Cotton and ZIF-67@CM Cotton fabrics, respectively. Further, after 1 h, adsorption values of 11.91 mg/g and 8.21 mg/g of anilines were observed in the two samples. However, after 2 h, the rate of adsorption was significantly slower. At the end of 12 h of exposure, the adsorption values were 18.15 mg/g and 12.66 mg/g, in the cases of ZIF-8@CM Cotton and ZIF-67@CM Cotton, respectively, which are about 400–600% higher than the control sample.

Interestingly, the adsorption of aniline was significantly higher in ZIF-8@CM Cotton compared to ZIF-67@CM Cotton. After 20 h, this value was 19.89 mg/g in ZIF-8@CM Cotton, which was ~35% higher compared to 14.41 mg/g in ZIF-67 @CM Cotton. As shown in Fig. 7(b) and (c), a similar adsorption trend was also observed with the two other aromatic pollutants, i.e., benzene and styrene. In the case of benzene, after 1 min, the ZIF-8@CM Cotton, ZIF-67@CM Cotton, and CM Cotton captured 2.41 mg/g, 2.69 mg/g, and 0.16 mg/g, respectively, of the aromatic pollutant. The initial rate of benzene adsorption in the two MOF functionalized fabrics was nearly the same (~12.4 mg/g) till 20 min.

However, after that, ZIF-8@CM Cotton exhibited a higher adsorption rate compared to ZIF-67@CM Cotton. After 1 h, the adsorption values of benzene increased to 15.26 mg/g, 13.71 mg/g, and 0.64 mg/g in the cases of ZIF-8@CM Cotton, ZIF-67@CM Cotton, and CM Cotton, respectively. Similar to the aniline adsorption, the CM Cotton fabric was observed to adsorb only 3.03 mg/g of benzene at saturation (after 20 h), while the ZIF-8@CM Cotton and ZIF-67@CM Cotton fabric captured 24.88 mg/g and 18.78 mg/g of benzene, respectively. It was very interesting to note that the control fabric, as well as the MOF functionalized fabrics, exhibited significantly lower adsorption of styrene. After 1 min, the adsorption values were 1.18 mg/g, 1.67 mg/g, and 0.07 mg/g in the cases of ZIF-8@CM Cotton, ZIF-67@CM Cotton, and CM Cotton, respectively. Further, after 1 h, these adsorption values increased to 6.24 mg/g, 4.34 mg/g, and 0.15 mg/g, respectively.

The adsorption trend of styrene reached near saturation in about 8 h. Afterward, a very small increase in adsorption was observed. The comparative maximum adsorption at saturation (after 20 h of exposure) of all the three pollutants on the control and MOF functionalized fabrics

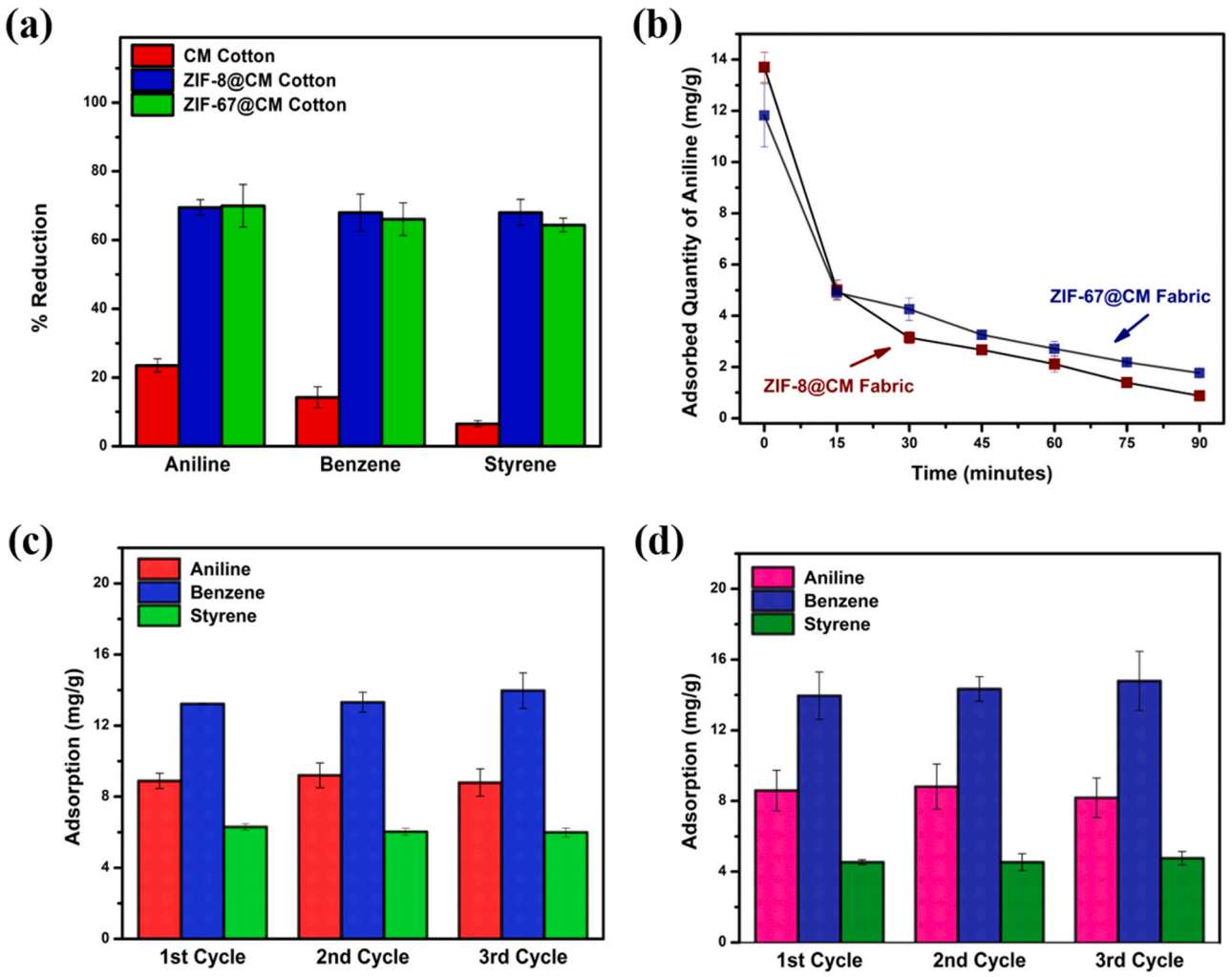

Fig. 9. (a) Bar graphs depicting the % reduction of aniline, benzene, and styrene by CM Cotton, ZIF-8@CM Cotton, and ZIF-67@CM Cotton fabric after 2 h at harmful environmental levels (500 ppm of each). (b) Desorption plot of aniline by ZIF-8@CM Cotton and ZIF-67CM Cotton fabric at 120 °C as a function of time. (c) Bar graphs illustrating the reusability of ZIF-8@CM Cotton fabrics for the adsorption of aniline, benzene, and styrene for three cycles. (d) Bar graphs showing the reusability of ZIF-67@CM Cotton for the adsorption of aniline, benzene, and styrene for three cycles.

is presented in Fig. 7d. The high concentration exposure experiments revealed that the MOF functionalized fabrics adsorb the model aromatic pollutants (aniline, benzene, and styrene) very rapidly during the initial stage of adsorption, and then the adsorption rates reduce significantly before saturation is attained. It is an expected trend, as initially, the MOF functional fabrics would have ample free sites to capture the aromatic pollutants. Once the pollutant molecules occupy some of these free sites, further adsorption becomes slow due to hindered diffusion and finally leads to saturation. It is worth noting that the ZIF-8@CM Cotton fabric adsorbed a significantly higher amount of aromatic pollutants as compared to the ZIF-67@CM Cotton despite the fact that the add-on of ZIF-67 was slightly higher compared to that of ZIF-8 (as shown in Fig. 6c). Also, the two fabrics did not show any significant difference in BET and Langmuir surface areas. The difference in the adsorption capacity of both the fabrics could be due to the higher total effective surface area of ZIF-8 MOFs as compared to the ZIF-67 MOFs, as shown in Fig. 6(d). Also, the ZIF-8 @CM Cotton fabric had a higher external surface area as compared to the ZIF-67@CM Cotton.

Further, to investigate the adsorption difference between ZIF-8@CM Cotton and ZIF-67@CM Cotton fabrics, the stability studies were performed by immersing the functionalized fabrics in water for 24 h. In the case of ZIF-8@CM Cotton fabric, there was a significant change in ZIF-8 peaks after the water treatment, as shown in Fig. 8(a). It may not be due to the instability or disintegration of ZIF-8 crystals because ZIF-8 crystals are stable in water up to several days, as shown by Zhou et al. (Zhou et al., 2017). It may be due to the detachment of some of the loosely held ZIF-8 crystals from the fabric in the presence of water. On the other hand, in the case of ZIF-67@CM Cotton fabrics, ZIF-67 crystals seem to have detached to a large extent from the fabric, as evident from the diminished peaks of ZIF-67 in XRD spectrum shown in Fig. 8(b). Zhou et al. have also shown that the ZIF-67 crystals are unstable in humid conditions. Since the water was used during the growth of MOFs on the fabric, it may be possible that small traces of water inside ZIF-67 pores or structures can lead to its structural disintegration with time and might be responsible for the lower surface area and adsorption capacity.

Among the three aromatic pollutants, the overall adsorption of benzene was observed to be highest for both the MOF functional fabrics, followed by aniline and styrene. The benzene has the smallest size among the three compounds studied. Its structure does not have any substitution on its aromatic rings. On the other hand, styrene has a $-CH=CH_2$ group, which makes styrene bulkier compared to aniline and benzene. The bulkiness and steric hindrance due to $-CH=CH_2$ group on

Table 2
Comparison of adsorption capacities of ZIF MOF functionalized fabrics with other absorbents.

Adsorbent	Aniline adsorption (mg/g)	Benzene adsorption (mg/g)	Styrene adsorption (mg/g)	Reference
MOF-520 (Al)		1007		(Gwardiak et al., 2019)
ZIF-8		570		(Gwardiak et al., 2019)
MIL-Z1 (Cr)		546		(Zhu et al., 2017)
MIL-101 (Cr)		294		(Xian et al., 2015)
Montmorillonite (Clay)		141.2		(Deng et al., 2017)
Activated Carbon	125.3	123.05	272.83	(C. Chen et al., 2017; Samaddar et al., 2019)
Halloysite (Clay)		68.1		(Deng et al., 2017)
Kaolinite (Clay)		56.7		(Deng et al., 2017)
ZIF-8 @CM Cotton	19.9	24.8	11.2	*
ZIF-67 @CM Cotton	14.4	18.8	5.4	*
ZIF-8 (based on % addition of ZIF-8 on fabric)	136	175.8	88.3	*
ZIF-67 (based on % addition of ZIF-67 on fabric)	81.4	112.1	37	*
CM Cotton	2.9	3.0	0.2	*

*Values obtained in the current study

styrene limits its adsorption on ZIF-8/ZIF-67@CM Cotton fabric, ultimately evident from its lowest adsorption value compared to that of aniline and benzene. Similarly, aniline also has -NH_2 group associated with its aromatic ring, which imparts less steric hindrance during adsorption than $-CH=CH_2$ group of styrene. Therefore, its adsorption value is higher compared to styrene. Finally, the benzene being the smallest, has the maximum adsorption on ZIF-8/ZIF-67 functionalized fabric. Additionally, these compounds were observed to adsorb in small amounts on CM Cotton. The observed adsorption values of benzene and aniline, which are similar, maybe the result of diffusion of these molecules inside the CM Cotton. On the other hand, styrene being the bulkiest may have limited diffusion.

In order to check the binding of adsorbed gases, the fabrics saturated with three aromatic pollutant gases were kept in an active vacuum for half an hour. Interestingly, the adsorbed pollutants did not diffuse out from the MOF functionalized fabric under vacuum. This indicates that the MOF functional fabrics can keep the pollutants attached to their surface until a suitable process is used for their extraction. Further, the adsorption experiments were performed by exposing the functionalized fabrics to harmful environmental concentrations (500 ppm) of pollutants to evaluate their performance in real-life conditions. As shown in Fig. 9(a), at 500 ppm concentration of pollutants, the MOF functionalized fabrics could successfully capture ~70% of all the three aromatic pollutants within 2 h. However, the control fabric (CM Cotton fabric), could adsorb only 23% of aniline, 14% of benzene, and 6.5% of styrene within 2 h. The experiments demonstrate the excellent potential of the MOF functionalized fabrics for the application of removal of aromatic VOCs from the ambient air.

In order to evaluate the reusability and regeneration of these stable MOF functionalized fabrics, the time-dependent desorption of aniline from the loaded MOF functionalized fabrics was studied at 120 °C. As shown in Fig. 9(b), after 15 min, the adsorbed aniline concentration decreased rapidly from 13.7 mg/g to 5 mg/g and 11.8–4.9 mg/g for the ZIF-8@CM Cotton and ZIF-67@CM Cotton, respectively. Interestingly, after 90 min, the aniline content was observed to be just 0.87 mg/g (for ZIF-8@CM Cotton) and 1.76 mg/g (for ZIF-67@CM Cotton). It was observed that the application of high temperatures resulted in nearly complete desorption of pollutants from both the MOF functionalized fabrics.

This suggests that these functionalized fabrics can be regenerated and may be suitable for repeated use. The shape of the desorption curve obtained also confirms the physisorption of aniline on the MOF functionalized fabric. The reusability of the MOF functional fabrics was investigated by regenerating the loaded fabrics by soaking them in methanol. The results are shown in Fig. 9(c) and (d) for ZIF-8@CM Cotton and ZIF-67@CM Cotton, respectively. The performance of MOF functionalized fabrics was evaluated for three cycles. Interestingly, for all the three cycles, the pollutant capture efficiency of the fabrics was observed to be nearly the same, confirming near-complete regeneration of MOF functionalized fabrics. The reusability experiments also confirmed the durability of the functionalized fabric and showed that MOFs did not detach or disintegrate on repeated use. Further, it was also observed that even after two AATCC 1 A washing cycles (i.e., 10 laundry washes), the fabric surface was uniformly covered with the MOFs. It showed that the reported fabrics are highly durable to harsh treatment during washing.

Table 2 presents the comparative analysis of the MOF functionalized fabrics with some standard adsorbents like activated carbon, clays, and MOFs. It may be observed that the values for MOF functionalized fabrics are lower than some of the other active compounds available in powder form. It may be noted that the main objective of the current research is to investigate an appropriate process/methodology to durably integrate MOF structures on flexible textile fabrics without the use of binders and without altering the feel and properties of the basic textile fabric. It was also intended to create a process that is based on an aqueous system using commercially viable steps. Further, the adsorption studies demonstrate that adequately porous MOF structures could be created using the adopted process. This integration enhances the handling and use of highly adsorbent materials such as MOFs in practical applications of functional filters, pollution controlling upholstery fabrics, etc. It has also been demonstrated that these functionalized fabrics can be regenerated and used repeatedly. On the other hand, the applications of various porous materials, such as clays, activated carbon, and MOFs, are limited due to their powdery nature and difficulty in handling. With regards to the adsorption capacity of MOFs on the fabric, it may be noted that even if other adsorbents such as clays, activated carbons, etc., were to be integrated using a binder, they would have shown possibly much lower adsorption values based on the weight of the functionalized fabric.

Further, they would have affected the feel, appearance, and reusability due to their poor integration and use of a binder, which would have blocked the access to the pores of active material. In this study, only about 12–14 wt% of MOFs on the weight of the fabric were integrated. This small amount could result in high adsorption values of 18–24 mg/g of fabric for benzene. Integration of other materials at this concentration would have resulted in similar or lower values for the reasons given above.

The table also presents the values of adsorption based on the weight of the MOFs on the fabric (i.e., excluding the fabric weight) to show the quality of MOFs developed on the fabric. Since these MOFs have been grown with chemical integration with the carboxymethyl groups present on the CM cotton, their porosity and structure are likely to be a little different. The higher value of 570 mg/g for benzene in ZIF-8 powder reported in the literature (Gwardiak et al., 2019) has been obtained using saturation vapor pressure at 0.1 atm, which eliminates the competition of benzene molecules with other gases (such as CO_2)/moisture present in the atmosphere and within MOFs. On the other hand, the value of 175 mg/g (based on ZIF-8 addon on the ZIF-8@CM cotton) has been obtained at standard room conditions (25–30 °C, 55–65% RH and atmospheric pressure) to simulate practical applications and is therefore quite high. CM Cotton values have been

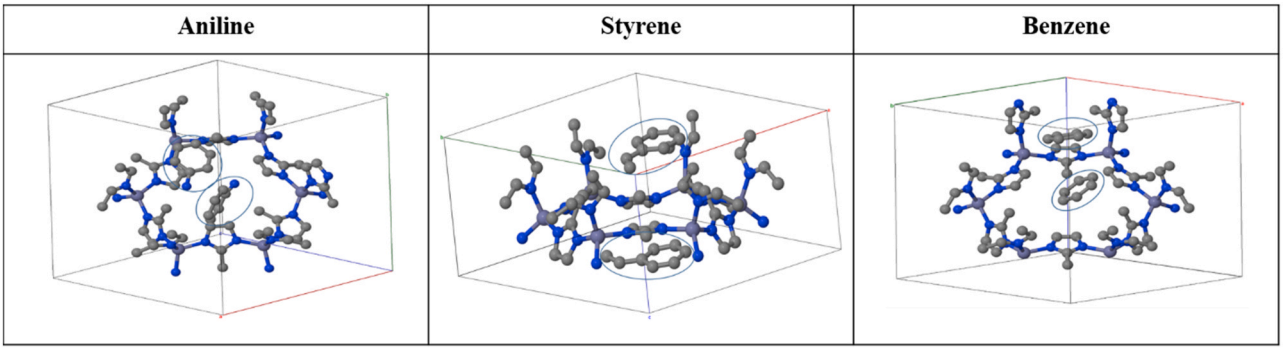

Fig. 10. Aromatic pollutants (aniline, styrene, and benzene) physisorbed on ZIF-8.

Table 3
Binding energies (BE) for the adsorption of aromatic pollutants on ZIF-8 and ZIF-67 at metallic and porous sites.

Model aromatic pollutants	Site	Binding energy (eV)	
		(ZIF-8)	(ZIF-67)
Aniline	Metallic site (Zn/Co)	−0.67	−0.69
	Porous site (Center)	−0.30	−0.44
Benzene	Metallic site (Zn/Co)	−0.58	−0.55
	Porous site (Center)	−0.13	−0.07
Styrene	Metallic site (Zn/Co)	−0.67	−0.71
	Porous site (Center)	−0.39	−0.44

shown to suggest that cotton by itself does not really participate in the adsorption of such pollutants.

3.3. Computational studies

DFT calculations were performed to investigate the adsorption behavior of aromatic pollutants on ZIF-8 and ZIF-67. The corresponding binding energies (BE) were calculated at the metallic sites (Zn and Co, respectively) and porous sites (i.e. at center).

The first-principle analyses (Fig. 10) indicated the presence of pi-pi interactions between the pollutants and the imidazole ring of the MOFs. The binding energies (BE) for the three aromatic pollutants for the two systems are listed in Table 3. The BE values of < 1 eV implied physisorption of the pollutants on the MOF structures. Further, the negative values of BE indicated the stability of the adsorbed pollutants, which implies that the pollutants are not likely to get desorbed without the application of external stimuli such as high temperature, washing with solvents, etc. These inferences support the experimental observations reported above. The application of vacuum could not result in the desorption of the model pollutants from the functionalized fabric as shown in section 3.2. However, the pollutants could be successfully desorbed on the application of heat, and the functionalized fabrics could be recycled/reused repeatedly.

Both ZIF-8 and ZIF-67 showed similar values of BE for the three pollutant molecules, which are also in agreement with the experimental observations. The BE values per pollutant ring, for the number of pollutant rings up to 5 in the system, have also been reported in Table S2 in the Supplementary Information. The interaction BE was found to be higher for metallic sites than for the pore sites in MOFs, which are in conformity with the reported literature (Wen et al., 2019).

Among the three model pollutants, benzene was observed to have somewhat lower BE than that of aniline and styrene. However, in the experiments, benzene was found to get adsorbed more than the other two. This suggests that the extent of adsorption is probably dominated by the lower steric hindrance provided by benzene molecules compared to the other two molecules, which have bulky side groups.

4. Conclusions

In this study, the functionalization of cotton fabric by ZIF MOFs (ZIF-8 and ZIF-67) has been demonstrated using a rapid, facile, eco-friendly, and scalable approach. The XRD, SEM, and EDX analyses confirmed the uniform growth of crystalline MOFs on the entire surface of the carboxymethylated cotton fabric. The functionalized fabrics exhibited a high specific surface area. The MOF functionalized fabrics could rapidly adsorb significantly high amounts of three model aromatic pollutants, namely aniline, benzene, and styrene. The ZIF-8 functionalized fabric could adsorb a maximum of 19.89 mg/g of aniline, 24.88 mg/g of benzene, and 11.16 mg/g of styrene on the weight of the fabric. The adsorbed gases could remain bound with the fabrics even under active vacuum conditions of $\sim$ 1 torr. However, these fabrics could be easily regenerated by heating the fabrics at 120 °C and reused without any decrease in their adsorption capacity for several cycles. ZIF-8 was found to have better stability than ZIF-67 under moist conditions. DFT studies confirmed the physisorption mechanism involving the pi-pi interactions between the pollutant and the imidazole ring of the ZIF compounds. All three model pollutants displayed similar binding energies. The ZIF functionalized textiles possess a huge potential for applications as protective garments and in controlling indoor air pollution.

CRediT authorship contribution statement

Hardeep Singh Jhinjer, Manjeet Jassal, Ashwini K. Agrawal: Planned and designed the research. **Hardeep Singh Jhinjer:** Performed the experiments. **Arunima Singh, Saswata Bhattacharya:** Planned the DFT studies. **Arunima Singh:** Performed the DFT calculations. **Manjeet Jassal, Ashwini K. Agrawal, Saswata Bhattacharya:** Reviewed and edited the manuscript. All the authors have approved the final version of the manuscript.

Declaration of Competing Interest

The authors declare that they have no known competing financial interests or personal relationships that could have appeared to influence the work reported in this paper.

Acknowledgments

The authors acknowledge partial financial support from various research grants provided by the Department of Science and Technology, Govt. of India and Resil Chemical Pvt. Ltd., Bengaluru under Nano mission. The authors would also like to acknowledge the use of characterization facilities provided by Nanoscale Research Facility (NRF), IIT Delhi, and computational resources provided by the High-Performance Computing (HPC) Facility, IIT Delhi.

Appendix A. Supporting information

Supplementary data associated with this article can be found in the online version at doi:10.1016/j.jhazmat.2021.125056.

References

Abdelhameed, R.M., Emam, H.E., Rocha, J., Silva, A.M., 2017. Cu-BTC metal-organic framework natural fabric composites for fuel purification. Fuel Process. Technol. 159, 306–312.

Chen, C., Geng, X., Huang, W., 2017. Adsorption of 4-chlorophenol and aniline by nanosized activated carbons. Chem. Eng. J. 327, 941–952. https://doi.org/10.1016/j.cej.2017.06.183.

Chen, Y., Li, S., Pei, X., Zhou, J., Feng, X., Zhang, S., Cheng, Y., Li, H., Han, R., Wang, B., 2016. A solvent-free hot-pressing method for preparing metal–organic-framework coatings. Angew. Chem. Int. Ed. 55, 3419–3423. https://doi.org/10.1002/anie.201511063.

Chen, Y., Zhang, S., Cao, S., Li, S., Chen, F., Yuan, S., Xu, C., Zhou, J., Feng, X., Ma, X., Wang, B., 2017. Roll-to-roll production of metal-organic framework coatings for particulate matter removal. Adv. Mater. 29, 1606221 https://doi.org/10.1002/adma.201606221.

Deng, L., Yuan, P., Liu, D., Annabi-Bergaya, F., Zhou, J., Chen, F., Liu, Z., 2017. Effects of microstructure of clay minerals, montmorillonite, kaolinite and halloysite, on their benzene adsorption behaviors. Appl. Clay Sci. 143, 184–191. https://doi.org/10.1016/j.clay.2017.03.035.

Emam, H.E., Abdelhameed, R.M., 2017. Anti-UV radiation textiles designed by embracing with nano-MIL (Ti, In)–metal organic framework. ACS Appl. Mater. Interfaces 9, 28034–28045. https://doi.org/10.1021/acsami.7b07357.

Furukawa, H., Cordova, K.E., O'Keeffe, M., Yaghi, O.M., 2013. The chemistry and applications of metal-organic frameworks. Science 341. https://doi.org/10.1126/science.1230444.

Gwardiak, S., Szczęśniak, B., Choma, J., Jaroniec, M., 2019. Benzene adsorption on synthesized and commercial metal–organic frameworks. J. Porous Mater. 26, 775–783. https://doi.org/10.1007/s10934-018-0678-0.

Hobday, C.L., Woodall, C.H., Lennox, M.J., Frost, M., Kamenev, K., Düren, T., Morrison, C.A., Moggach, S.A., 2018. Understanding the adsorption process in ZIF-8 using high pressure crystallography and computational modelling. Nat. Commun. 9, 1429. https://doi.org/10.1038/s41467-018-03878-6.

Hohenberg, P., Kohn, W., 1964. Inhomogeneous electron gas. Phys. Rev. 136, B864–B871. https://doi.org/10.1103/PhysRev.136.B864.

Hu, Y., Liu, Z., Xu, J., Huang, Y., Song, Y., 2013. Evidence of pressure enhanced CO_2 storage in ZIF-8 probed by FTIR spectroscopy. J. Am. Chem. Soc. 135, 9287–9290. https://doi.org/10.1021/ja403635b.

Kampa, M., Castanas, E., 2008. Human health effects of air pollution. Environ. Pollut., Proc. 4th Int. Workshop Biomonit. Atmos. Pollut. (Emphas. Trace Elem.) 151, 362–367. https://doi.org/10.1016/j.envpol.2007.06.012.

Knebel, A., Geppert, B., Volgmann, K., Kolokolov, D.I., Stepanov, A.G., Twiefel, J., Heitjans, P., Volkmer, D., Caro, J., 2017. Defibrillation of soft porous metal-organic frameworks with electric fields. Science 358, 347–351. https://doi.org/10.1126/science.aal2456.

Kohn, W., Sham, L.J., 1965. Self-consistent equations including exchange and correlation effects. Phys. Rev. 140, A1133–A1138. https://doi.org/10.1103/PhysRev.140.A1133.

Kolokolov, D.I., Stepanov, A.G., Jobic, H., 2015. Mobility of the 2-methylimidazolate linkers in ZIF-8 probed by 2H NMR: saloon doors for the guests. J. Phys. Chem. C 119, 27512–27520. https://doi.org/10.1021/acs.jpcc.5b09312.

Kresse, G., Furthmüller, J., 1996. Efficient iterative schemes for ab initio total-energy calculations using a plane-wave basis set. Phys. Rev. B 54, 11169–11186. https://doi.org/10.1103/PhysRevB.54.11169.

Krokidas, P., Castier, M., Economou, I.G., 2017. Computational study of ZIF-8 and ZIF-67 performance for separation of gas mixtures. J. Phys. Chem. C 121, 17999–18011. https://doi.org/10.1021/acs.jpcc.7b05700.

Kuma, P., Dereces, T., Etmek, T., Kolay, N., 2018. An easy and accurate method for determining degree of substitution on carboxymethylated cotton fabric. TEKSTİL ve KONFEKSİYON 7.

Lashaki, M.J., Fayaz, M., Wang, H. (Helena), Hashisho, Z., Philips, J.H., Anderson, J.E., Nichols, M., 2012. Effect of adsorption and regeneration temperature on irreversible adsorption of organic vapors on beaded activated carbon. Environ. Sci. Technol. 46, 4083–4090. https://doi.org/10.1021/es3000195.

Liu, J., Chen, L., Cui, H., Zhang, J., Zhang, L., Su, C.-Y., 2014. Applications of metal–organic frameworks in heterogeneous supramolecular catalysis. Chem. Soc. Rev. 43, 6011–6061. https://doi.org/10.1039/C4CS00094C.

Li, B., Chrzanowski, M., Zhang, Y., Ma, S., 2016. Applications of metal-organic frameworks featuring multi-functional sites. Coord. Chem. Rev. Chem. Appl. Met. Org. Framew. 307, 106–129. https://doi.org/10.1016/j.ccr.2015.05.005.

Li, J., Lu, R., Dou, B., Ma, C., Hu, Q., Liang, Y., Wu, F., Qiao, S., Hao, Z., 2012. Porous graphitized carbon for adsorptive removal of benzene and the electrothermal regeneration. Environ. Sci. Technol. 46, 12648–12654. https://doi.org/10.1021/es303069j.

López-Maya, E., Montoro, C., Rodríguez-Albelo, L.M., AznarCervantes, S.D., Lozano-Pérez, A.A., Cenís, J.L., Barea, E., Navarro, J.A.R., 2015. Textile/metal–organic-framework composites as self-detoxifying filters for chemical-warfare agents. Angew. Chem. Int. Ed. 54, 6790–6794. https://doi.org/10.1002/anie.201502094.

Lu, G., Hupp, J.T., 2010. Metal−organic frameworks as sensors: a ZIF-8 based Fabry−Pérot device as a selective sensor for chemical vapors and gases. J. Am. Chem. Soc. 132, 7832–7833. https://doi.org/10.1021/ja101415b.

Lu, L., Hu, C., Zhu, Y., Zhang, H., Li, R., Xing, Y., 2018. Multi-functional finishing of cotton fabrics by water-based layer-by-layer assembly of metal–organic framework. Cellulose 25, 4223–4238. https://doi.org/10.1007/s10570-018-1838-8.

Lu, A.X., McEntee, M., Browe, M.A., Hall, M.G., DeCoste, J.B., Peterson, G.W., 2017. MOFabric: electrospun nanofiber mats from PVDF/UiO-66-NH2 for chemical protection and decontamination. ACS Appl. Mater. Interfaces 9, 13632–13636. https://doi.org/10.1021/acsami.7b01621.

Neufeld, M.J., Harding, J.L., Reynolds, M.M., 2015. Immobilization of metal–organic framework copper(II) benzene-1,3,5-tricarboxylate (CuBTC) onto cotton fabric as a nitric oxide release catalyst. ACS Appl. Mater. Interfaces 7, 26742–26750. https://doi.org/10.1021/acsami.5b08773.

Nordin, N. a H.M., Ismail, A.F., Mustafa, A., Goh, P.S., Rana, D., Matsuura, T., 2014. Aqueous room temperature synthesis of zeolitic imidazole framework 8 (ZIF-8) with various concentrations of triethylamine. RSC Adv. 4, 33292–33300. https://doi.org/10.1039/C4RA03593C.

Pan, Y., Lai, Z., 2011. Sharp separation of C2/C3 hydrocarbon mixtures by zeolitic imidazolate framework-8 (ZIF-8) membranes synthesized in aqueous solutions. Chem. Commun. 47, 10275–10277. https://doi.org/10.1039/C1CC14051E.

Perdew, J.P., Burke, K., Ernzerhof, M., 1996. Generalized gradient approximation made simple. Phys. Rev. Lett. 77, 3865–3868. https://doi.org/10.1103/PhysRevLett.77.3865.

Phan, A., Doonan, C.J., Uribe-Romo, F.J., Knobler, C.B., O'Keeffe, M., Yaghi, O.M., 2010. Synthesis, structure, and carbon dioxide capture properties of zeolitic imidazolate frameworks. Acc. Chem. Res. 43, 58–67. https://doi.org/10.1021/ar900116g.

Phys. Rev. B 50, 17953 (1994) − Projector augmented-wave method, n.d. [WWW Document], URL ⟨https://journals.aps.org/prb/abstract/10.1103/PhysRevB.50.17953⟩ (accessed 5.7.20).

Rubin, H.N., Neufeld, B.H., Reynolds, M.M., 2018. Surface-anchored metal–organic framework–cotton material for tunable antibacterial copper delivery. ACS Appl. Mater. Interfaces 10, 15189–15199. https://doi.org/10.1021/acsami.7b19455.

Saini, V.K., Pires, J., 2017. Development of metal organic framework-199 immobilized zeolite foam for adsorption of common indoor VOCs. J. Environ. Sci. 55, 321–330. https://doi.org/10.1016/j.jes.2016.09.017.

Samaddar, P., Kim, K.-H., Yip, A.C.K., Zhang, M., Szulejko, J.E., Khan, A., 2019. The unique features of non-competitive vs. competitive sorption: Tests against single volatile aromatic hydrocarbons and their quaternary mixtures. Environ. Res. 173, 508–516. https://doi.org/10.1016/j.envres.2019.03.046.

da Silva Pinto, M., Sierra-Avila, C.A., Hinestroza, J.P., 2012. In situ synthesis of a Cu-BTC metal–organic framework (MOF 199) onto cellulosic fibrous substrates: cotton. Cellulose 19, 1771–1779.

Soni, V., Singh, P., Shree, V., Goel, V., 2018. Effects of VOCs on human health. In: Sharma, N., Agarwal, A.K., Eastwood, P., Gupta, T., Singh, A.P. (Eds.), Air Pollution and Control. Springer Singapore, Singapore, pp. 119–142. https://doi.org/10.1007/978-981-10-7185-0_8.

Takeuchi, M., Hidaka, M., Anpo, M., 2012. Efficient removal of toluene and benzene in gas phase by the TiO2/Y-zeolite hybrid photocatalyst. J. Hazard. Mater. 237–238, 133–139. https://doi.org/10.1016/j.jhazmat.2012.08.011.

Tkatchenko, A., Scheffler, M., 2009. Accurate molecular Van Der Waals interactions from ground-state electron density and free-atom reference data. Phys. Rev. Lett. 102, 073005 https://doi.org/10.1103/PhysRevLett.102.073005.

Tran, U.P.N., Le, K.K.A., Phan, N.T.S., 2011. Expanding applications of metal−organic frameworks: zeolite imidazolate framework ZIF-8 as an efficient heterogeneous catalyst for the knoevenagel reaction. ACS Catal. 1, 120–127. https://doi.org/10.1021/cs1000625.

Tu, M., Wannapaiboon, S., Khaletskaya, K., Fischer, R.A., 2015. Engineering Zeolitic-Imidazolate framework (ZIF) thin film devices for selective detection of volatile organic compounds. Adv. Funct. Mater. 25, 4470–4479. https://doi.org/10.1002/adfm.201500760.

Vellingiri, K., Kumar, P., Deep, A., Kim, K.-H., 2017. Metal-organic frameworks for the adsorption of gaseous toluene under ambient temperature and pressure. Chem. Eng. J. 307, 1116–1126. https://doi.org/10.1016/j.cej.2016.09.012.

Wang, C.-M., Chang, K.-S., Chung, T.-W., Wu, H., 2004. Adsorption equilibria of aromatic compounds on activated carbon, silica gel, and 13X zeolite. J. Chem. Eng. Data 49, 527–531. https://doi.org/10.1021/je0302102.

Wen, M., Li, G., Liu, H., Chen, J., An, T., Yamashita, H., 2019. Metal–organic framework-based nanomaterials for adsorption and photocatalytic degradation of gaseous pollutants: recent progress and challenges. Environ. Sci. Nano 6, 1006–1025. https://doi.org/10.1039/C8EN01167B.

Xian, S., Yu, Y., Xiao, J., Zhang, Z., Xia, Q., Wang, H., Li, Z., 2015. Competitive adsorption of water vapor with VOCs dichloroethane, ethyl acetate and benzene on MIL-101(Cr) in humid atmosphere. RSC Adv. 5, 1827–1834. https://doi.org/10.1039/C4RA10463C.

Yang, J., Zhang, F., Lu, H., Hong, X., Jiang, H., Wu, Y., Li, Y., 2015. Hollow Zn/Co ZIF particles derived from core–shell ZIF-67@ZIF-8 as selective catalyst for the semi-hydrogenation of acetylene. Angew. Chem. Int. Ed. 54, 10889–10893. https://doi.org/10.1002/anie.201504242.

Zhang, Y., Yuan, S., Feng, X., Li, H., Zhou, J., Wang, B., 2016. Preparation of nanofibrous metal–organic framework filters for efficient air pollution control. J. Am. Chem. Soc. 138, 5785–5788. https://doi.org/10.1021/jacs.6b02553.

Zhou, H.-C., Long, J.R., Yaghi, O.M., 2012. Introduction to metal–organic frameworks. Chem. Rev. 112, 673–674. https://doi.org/10.1021/cr300014x.

Zhou, K., Mousavi, B., Luo, Z., Phatanasri, S., Chaemchuen, S., Verpoort, F., 2017. Characterization and properties of Zn/Co zeolitic imidazolate frameworks vs. ZIF-8 and ZIF-67. J. Mater. Chem. A 5, 952–957. https://doi.org/10.1039/C6TA07860E.

Zhou, X., Tian, J., Hu, J., Li, C., 2018. High rate magnesium–sulfur battery with improved cyclability based on metal–organic framework derivative carbon host. Adv. Mater. 30, 1704166 https://doi.org/10.1002/adma.201704166.

Zhu, M., Hu, P., Tong, Z., Zhao, Z., Zhao, Z., 2017. Enhanced hydrophobic MIL(Cr) metal-organic framework with high capacity and selectivity for benzene VOCs capture from high humid air. Chem. Eng. J. 313, 1122–1131. https://doi.org/10.1016/j.cej.2016.11.008.

Zhu, Q., Tang, X., Feng, S., Zhong, Z., Yao, J., Yao, Z., 2019. ZIF-8@SiO2 composite nanofiber membrane with bioinspired spider web-like structure for efficient air pollution control. J. Membr. Sci. 581, 252–261. https://doi.org/10.1016/j.memsci.2019.03.075.